Eur. Phys. J. B **13**, 429–436 (2000)

**THE EUROPEAN PHYSICAL JOURNAL B**

EDP Sciences


# Optical properties and temperature dependence of critical transitions in ZnSe

R. Granger[1], J.T. Benhlal[1,a], O. Ndap[2], and R. Triboulet[2]

[1] Laboratoire de Physique des Solides, INSA, CS 14315, 35043 Rennes Cedex, France
[2] Laboratoire de Physique des Solides, CNRS, 92195 Meudon Cedex, France

Received 5 February 1999 and Received in final form 15 June 1999

**Abstract.** The dielectric function $\varepsilon$ of ZnSe has been deduced from ellipsometric measurements between 20 K and 380 K. $\varepsilon$ is analysed around each critical point with the standard critical point model. The variations of the different parameters characterising each transition with temperature are presented and analysed. The temperature coefficients of the energies of the critical transitions are given. $\varepsilon$ is essentially governed by the Coulomb interaction near the fundamental gap. Thanks to the high binding energy of the exciton and the low spectral width of the ellipsometer, the fundamental state of the exciton is found completely separated from the first excited states and the continuum at low temperature. In return the strong transition $E_1$ near the L points of the Brillouin zone can be described equally well with a 2D or an excitonic transition.

**PACS.** 78.40.Fy Semiconductors – 78.20.Ci Optical constants (including refractive index, complex dielectric constant, absorption, reflection and transmission coefficients, emissivity) – 71.20.Nr Semiconductor compounds

## 1 Introduction

ZnSe is a wide gap II-VI semiconductor which appeared promising for the elaboration of blue light emitters in the beginning of the nineties [1,2]. Despite the relatively low defect densities of the related compounds used in the device elaboration the lifetime of these II-VI blue lasers remains still too short to reach the industrial step. Now nitrides appear to be of better value for this type of applications. However ZnSe remains a technological material for optical devices as it has a broad transparency spectrum. Its use in optical devices is interesting as its dielectric function appears insensitive to defect densities or to growth methods. Very accurate measurements of the ZnSe refractive index $n$, performed in 1979 [3] and 1990 [4] on samples grown independently, show variations which are inside measurement uncertainties ($\sim 2 \times 10^{-4}$ in absolute value). There is a great amount of optical data of ZnSe which are mainly gathered in references [5,6]. Since these reviews the room temperature dielectric function ($\varepsilon = \varepsilon_\mathrm{r} + \mathrm{i}\varepsilon_\mathrm{i}$) of ZnSe has been deduced from ellipsometric measurements and described with a model dielectric function (MDF) by Adachi and Taguchi [7]. Recently Kim and Sivanathan gave $\varepsilon$ data of ZnSe grown epitaxially on GaAs [8]. Moreover they use a more elaborated MDF model [9] to describe spectral variations of $\varepsilon$ with a great precision. They show that the excitonic contribution must be taken into account to describe $\varepsilon$ in the vicinity of the fundamental gap at room temperature as the exciton binding energy ($\cong$ 19 meV [5]) is large for this semiconductor.

Reflectivity measurements show an asymmetry of $\varepsilon_\mathrm{i}$ around critical transitions of higher energies [10]. ZnSe dielectric function $\varepsilon$ was described with different models [7,9]. Though we are able to use the MDF of Kim *et al.* [11], we will use the standard critical point (SCP) description [12] in order to obtain an information on the type of transitions through the evolution, with temperature, of the parameters entering this description. In such a study the type of transition is in fact the only choice. The phase angle $\phi$, which will be defined later, relates mainly to the asymmetry of $\varepsilon$ around a critical point. Its variations with temperature will give informations on the transitions considered.

This paper presents, for the first time, a comprehensive set of experimental variations of the dielectric function of bulk ZnSe as measured with spectroscopic ellipsometry (SE) between 20 K and 380 K. The corresponding results are analysed with the SCP model to characterise critical transitions. The paper is organised as follows: Section 2 gives the necessary details about material growth, sample preparation and ellipsometric measurements at low temperature. Section 3 presents $\varepsilon$ measurements and their analysis. SCP parameters of each transition are given as a function of temperature and are critically studied in Section 4 which is followed by the conclusion.

[a] e-mail: jamal.benhlal@insa-rennes.fr

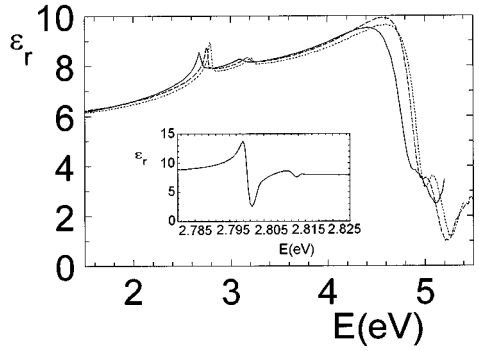


**Fig. 1.** Real part $\varepsilon_{\rm r}$ of the ZnSe dielectric function at (——) 20 K, (— — —) 145 K (—) 292 K. The inset gives a blowup of $\varepsilon_{\rm r}$ around the fundamental gap at 20 K.

## 2 Material growth, sample surface preparation and low temperature measurements

Monocrystals of ZnSe are obtained by solid phase recrystallization of polycrystalline boules during an annealing treatment in the 1000-1100 °C temperature range, under a high selenium pressure and during about 20 days [13]. Photoluminescence and diffraction experiments show a very high quality material [14]. The sample process preparation is detailled in reference [33]. Our value $\varepsilon_{\rm i}(E_1)$ reaches 11.6. This value is higher than those given in references [7,15] but, however, slightly less than 12 given in reference [8]. Ellipsometric measurements are performed with a phase modulated spectroscopic ellipsometer UVISEL (Instrument S.A.). The measurements are usually done in steps of 10 meV except in the vicinity of the fundamental gap $E_0$ where it is decreased from 5 meV at room temperature to 0.5 meV at 20 K. The ellipsometer gives the ellipsometric angles $\Psi$ and $\Delta$ which are defined by the ratio $r_{\rm p}/r_{\rm s} = \tan\Psi {\rm e}^{{\rm i}\Delta}$ where $r_{\rm p}$ and $r_{\rm s}$ are the complex reflectivities for polarisation of the light parallel and perpendicular to the plane of incidence [16]. The value of $\varepsilon$ is easily deduced if there is no overlayer on the sample surface. When $\varepsilon_{\rm i}(E_1)$ has reached its maximum value (11.6), $\varepsilon$ is monitored at room temperature (292 K) from 0.7 eV to 5.5 eV. Then, the sample is placed on the cold finger of a ultrahigh vacuum cryostat with strain free silica windows [17]. The cryostat is evacuated with turbomolecular pumps and baked up to 160 °C to reach a pressure lower than $10^{-7}$ Pa at room temperature. This low pressure is necessary to avoid gas condensation on the sample at low temperature [17]. The sample temperature is adjusted from 20 K to 380 K with an uncertainty of 0.2 K below 150 K and 0.5 K up to 380 K.

## 3 Ellipsometric measurements and dielectric function analysis

Ellipsometric measurements are performed at an angle of incidence of 71°. After each change of the sample temperature, the optical alignment is checked and a new polarisation calibration is performed to take into account the possible polarisation of the windows as the optical beams can be not strictly perpendicular to them.

The ellipsometric angles are monitored again with the sample in the cryostat at 292 K. Then the composition of the overlayer which has naturally grown on ZnSe during the transfer of the sample to the cryostat is deduced. So the complex refractive index of this layer $\tilde{n} = n + {\rm i}k$ is described by the phenomenological expression of Sellmeier for absorbing materials [34].

$$n^2 = (1+A)(1+B/\lambda^2)^{-1}, k = C(nD\lambda + J/\lambda + 1/\lambda^3)^{-1} \quad (1)$$

where $\lambda$ is the wavelength of the light and $A$, $B$, $C$, $D$ and $J$ are real constants. The pseudo dielectric function of the ZnSe sample placed in the cryostat is very well fitted when the parameters defined in (1) take the values given in Table 1. The thickness of the overlayer is very small (0.49 nm) so the uncertainty of the estimation of its dielectric function is high since this value is in the order of the roughness depth. This effective dielectric function of the overlayer and its thickness are assumed to be independent on temperature $T$ [19]. For each temperature $\varepsilon$ is corrected from the contribution of the overlayer to obtain the dielectric function of ZnSe.

Figures 1 and 2 show $\varepsilon_{\rm r}$ and $\varepsilon_{\rm i}$ spectra of ZnSe for some selected temperatures. The critical transitions are located by arrows in Figure 2. They are named, by decreasing energy, $E_1+\Delta$, $E_1$, $E_0+\Delta_0$, and $E_0$. The insets of Figures 1 and 2 show enlargements of $\varepsilon_{\rm r}$ and $\varepsilon_{\rm i}$ in the vicinity of the fundamental gap $E_0$. In this spectral domain the dielectric response is obviously dominated by the exciton [12], at least at low temperatures. The states $1s$, $2s$ and $3s$ of

**Table 1.** Thickness and values of parameters entering relation (1) describing the dielectric function of the overlayer on the ZnSe surface (*cf.* Fig. 2).

| $d$ (nm) | $A$ | $10^{-4}B$ $(\text{nm})^2$ | $10^3C$ | $10^2D$ $(\text{nm})^{-1}$ | $10^{-2}J$ (nm) |
|---|---|---|---|---|---|
| 0.49 | 0.308 | 5.9 | 6 | 0.25 | 0.9 |
| ±0.007 | ±0.005 | ±0.09 | ±0.0004 | ±0.01 | ±0.03 |

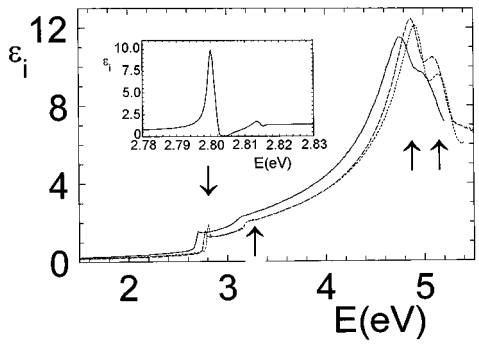


**Fig. 2.** Imaginary part $\varepsilon_{\rm i}$ of the ZnSe dielectric function with the same symbol meanings as in Figure 3.

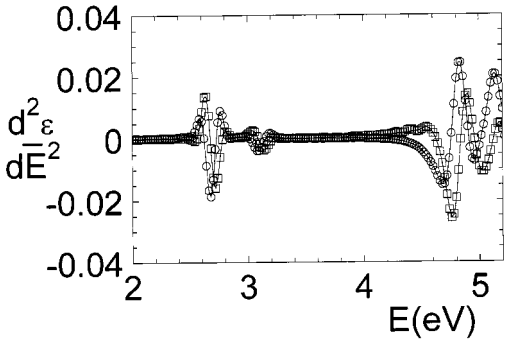


**Fig. 3.** Example of second derivatives at 300 K of (○) $\varepsilon_r$ and of (□) $\varepsilon_i$ with their fit with exciton lineshapes for all transitions.

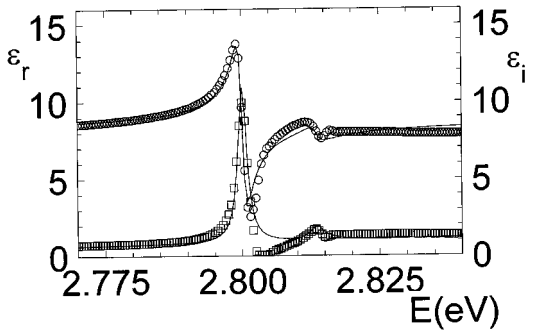


**Fig. 4.** Experimental data on $\varepsilon_r$ (○) and $\varepsilon_i$ (□) near the fundamental gap at 20 K with their fit with relations (3)+(2) and taking into account of the spectral width of the monochromator.

the exciton are clearly visible on the $\varepsilon_r$ and $\varepsilon_i$ spectra. The inset of Figure 2 shows that $\varepsilon_i$ goes to a non measurable value above the first exciton state. To our knowledge this is the first time that ellipsometric experimental data reveals the fundamental state of the exciton completely separated from its excited states and the continuum. This is due to the high binding energy of the exciton ($\cong$ 19 meV [23]), to the high quality of the crystal and to the relatively high resolution of the monochromator of the ellipsometer which has of focal length of 0.640 m. Its spectral width is decreased to 0.5 meV. The use of lower widths degrades the signal to noise ratio in the monitoring of $\psi$ and $\Delta$ values leading to poorer $\varepsilon(E)$ data and fits. No other features have been evidenced above the three first exciton states at low temperatures. The discussion on the analysis of $\varepsilon$ near $E_0$ will be given below.

The analysis of $\varepsilon(E)$ follows the usual SCP model. Around a critical point of energy $E_\ell$, the local dielectric constant $\varepsilon_\ell$ is described by the general expression [20]:

$$\varepsilon_\ell(E) = C_\ell \Gamma_\ell^{-n} e^{i\Phi_\ell}(E - E_\ell + i\Gamma_\ell)^n + F(E) \qquad (2)$$

$\Gamma_\ell$ is the broadening parameter, $C_\ell\Gamma_\ell^{-n}$ the oscillator strength and $n$ is the order of the transition ($n = 1/2$ for a 3D transition, $n = 0$ (logarithmic) for a 2D transition, $n = -1/2$ for a 1D transition and $n = -1$ for a discrete exciton). $F(E)$ is a slowly varying function of $E$ coming from remote transitions; its derivatives are usually assumed to be negligible [20]. $\Phi_\ell$ is a phase whose value is a multiple of $\pi/2$ for transitions between uncorralated electron states. Other values of $\Phi_\ell$ are attributed to a mixture of contiguous SCP due to correlation effects [12].

For each critical transition, the parameters defined in (2) are adjusted by fitting simultaneously the second derivatives of experimental $\varepsilon_r(E)$ and $\varepsilon_i(E)$ to those of the real and imaginary parts of $\varepsilon_\ell(E)$. A slight smoothing with an exponential regression is applied after the first and the second differentiation of the experimental data in the analysis of the weak transition $E_0 + \Delta_0$ for temperatures above 120 K. To avoid possible distortions in numerical calculations, the lineshapes given by (2) are also numerically calculated and, if necessary, smoothed with the same procedures as those applied to calculate the second derivatives of $\varepsilon_r$ and $\varepsilon_i$ [21]. The fit is performed with the Levenberg-Marquart method [22]. $E_1$ and $E_1 + \Delta_1$ transitions are fitted simultaneously as they are adjoining. For $E_0 + \Delta_0$ and $E_0$ the contributions of the two upper transitions to the second derivatives of $F(E)$ in (2) are also taken into account.

An example of the second derivatives of $\varepsilon_r(E)$ and $\varepsilon_i(E)$ is given in Figure 3. This figure shows that, in the vicinity of critical points, relation (2) gives a good description of $\varepsilon(E)$. However Figure 3 corresponds to a sample temperature where the discrete contributions of the exciton have disappeared and the above mentioned fit of the lineshapes given by (2) can be applied. Below 200 K the discrete structures due to the exciton are clearly seen and their contribution to $\varepsilon$ must be added to those of the continuum which extends above $E_0$. They are written according to [24] as:

$$\varepsilon_{Ex}(E) = \sum_{p=1}^{3} \frac{1}{p^3[E - (E_0 - G/n^2) + i\Gamma_{Ex,p}]} \qquad (3)$$

where $G$ is the exciton binding energy, $\Gamma_{Ex,p}$ the broadening parameter associated to state $p$, each $\Gamma_{Ex,p}$ is left free in the fit. The sum is limited to $p = 3$ as only three peaks are resolved in the $\varepsilon$ spectra below $E_0$. The contribution of the continuum above $p = 3$ is cast up in that of the critical point $E_0$ which is given by (2) with $n = 1/2$. The deviation from an ideal 3D $M_0$ transition due to this continuum is taken into account through the phase term $\Phi(E_0)$ in (2). The fit of the sum of (2) + (3) is performed directly on $\varepsilon_r$ and $\varepsilon_i$ data and not through their derivatives. The small spectral width of the exciton lines allows to obtain a good fit. Moreover the number of values of $\varepsilon_r(E)$ and $\varepsilon_i(E)$ included in each of the exciton lines is small creating strong distortions in the calculation of the derivatives.

Figure 4 shows the result of the simultaneous fit of $\varepsilon_r$ and $\varepsilon_i$ data with the discrete contribution of the exciton and that of the continuum of a 3D critical point. The spectral range of the fit is limited above $E_0$ to stay in the constant effective mass approximation of the SCP model.

**Table 2.** Optical transitions in ZnSe, their location in the Brillouin zone, their symmetry and their calculated energy from [27].

| Critical point | Location | Symmetry | 0 K energy (eV) |
|---|---|---|---|
| $E_0$ | $\Gamma_8^{\rm V} \rightarrow \Gamma_6^{\rm c}$ | $M_0$ | 2.76 |
| $E_0 + \Delta_0$ | $\Gamma_7^{\rm V} \rightarrow \Gamma_6^{\rm c}$ | $M_0$ | 3.21 |
| $E_1$ | $\Gamma_{4.5}^{\rm V} \rightarrow \Gamma_6^{\rm c}$ | $M_1$ | 4.72 |
| $E_1 + \Delta_1$ | $\Gamma_6^{\rm V} \rightarrow \Gamma_6^{\rm c}$ | $M_1$ | 5.00 |

## 4 Results and their analyses

ZnSe is a direct gap semiconductor, the distribution of the electronic states in the Brillouin zone is of the same type as those of other direct gap III-V and II-VI compounds. Drawings of the bands can be found in references [7] or [27] and are not recalled here. Table 2 recalls the critical transitions with their energies and their symmetries which are found in the spectral domain where $\varepsilon$ is measured. The results are now examined for each of these transitions.

The values of the parameters of a transition defined in (2) depends on the type of lineshape chosen for the fit. The type of lineshape used is indicated with a suffix placed in parentheses at the end of the letters designing the parameter. Ex labels the excitonic lineshape.

The variations of the energies of the critical transitions with temperature are given in Figures 5a and 5b. The decrease of the electronic states energies with $T$ comes from two contributions [25]: the first originates from the thermal expansion of the lattice and the second is due to thermal vibrations of the lattice which spread the atomic potentials. The $E_\ell(T)$ are naturally described with Bose-Einstein relations of the type [17,19]:

$$E_\ell(T) = E_{\ell 0} - \alpha_\ell \left[1 + \frac{2}{{\rm e}^{T_\ell/T} - 1}\right] \qquad (4)$$

where $E_{\ell 0}$, $\alpha_\ell$ and $T_\ell$ are adjustable parameters. $T_\ell$ is an effective temperature which is related to the excitation of phonons interacting with the electronic states considered. The values of the parameters deduced from the fit of $E_\ell(T)$ are given in Table 3. $E_\ell(T)$ variations become almost linear above 100 K. Mean temperature coefficients $\mathrm{d}E_\ell/\mathrm{d}T|_m$ are calculated from results between 100 K and 300 K. Their values are given in Table 4 with those already published. When $E_\ell(T)$ data are fitted with expression (4), a high temperature limit of $\mathrm{d}E_\ell/\mathrm{d}T$ is given by $\mathrm{d}E_\ell/\mathrm{d}T|_{\rm h} = -2\alpha_\ell/T_\ell$. This value is also reported in Table 4.

The variations of the Lorentzian broadening parameters $\Gamma_\ell$ with $T$ are gathered in Figures 6a and 6b. They are also described with an expression similar to (4) [17,19]:

$$\Gamma_\ell(T) = \Gamma_{\ell 1} + \Gamma_{\ell 0} \left[1 + \frac{2}{{\rm e}^{T_\ell/T} - 1}\right] \qquad (5)$$

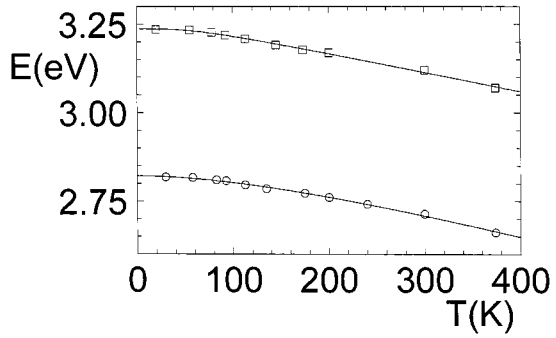


(a)

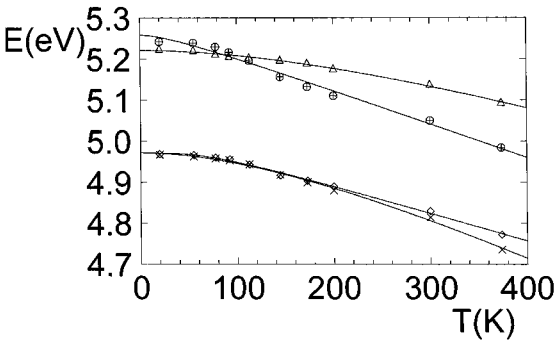


(b)

**Fig. 5.** (a) Temperature variation of ($\circ$) $E_0$ and ($\square$) $E_0 + \Delta_0$ both deduced with an exciton lineshape. Full lines correspond to fits with relation (3). (b) Temperature variations of ($\Diamond$) $E_1$, ($\oplus$) $E_1 + \Delta_1$, deduced with an exciton lineshape; ($\times$) $E_1$, ($\triangle$) $E_1 + \Delta_1$ deduced with a 2D lineshape.

**Table 3.** Values of the parameters entering relation (4) giving the energy of critical transitions *versus* temperature. The last suffix in column 1 indicates the lineshape used for the fit of experimental data.

| Transition $\ell$ and fitting lineshape | $E_{\ell 0}$ (eV) | $\alpha_\ell$ (meV) | $T_\ell$ (K) | Error bar on $E_\ell$ (meV) |
|---|---|---|---|---|
| $E_0$ | 2.887 | 70 | 248 | $\pm 3$ |
| $(E_0 + \Delta_0)_{\rm Ex}$ | 3.283 | 47 | 171 | $\pm 5$ |
| $(E_1)_{\rm 2D}$ | 5.082 | 116 | 267 | $\pm 9$ |
| $(E_1)_{\rm Ex}$ | 5.038 | 67 | 195 | $\pm 6$ |
| $(E_1 + \Delta_1)_{\rm 2D}$ | 5.285 | 67 | 280 | $\pm 6$ |
| $(E_1 + \Delta_1)_{\rm Ex}$ | 5.290 | $\pm 0.0466$ | $+99$ | $\pm 10$ |

$T_\ell$ is different from $T_\ell$ of (4) as only thermal vibrations contribute to $\Gamma_\ell$. The values of the parameters defined in (5) are given in Table 5.

### 4.1 $E_0$ transition

This transition, corresponding to the fundamental gap, involves the $\Gamma_8^{\rm v}$ valence band state and the $\Gamma_6^{\rm c}$ conduction band state in the double group notation. The three first states of the exciton are clearly visible (*cf.* inset of

**Table 4.** Temperature coefficients of critical transitions (in $10^4$ eV K$^{-1}$), the subscript meanings are: h, high temperature limit; m, as deduced between 100 and 300 K; d, other experimental determinations with the reference.

| Transition $\ell$ and fitting lineshape | $-\left.\frac{\mathrm{d}E_\ell}{\mathrm{d}T}\right\|_\mathrm{h}$ | $-\left.\frac{\mathrm{d}E_\ell}{\mathrm{d}T}\right\|_\mathrm{m}$ | $-\left.\frac{\mathrm{d}E_\ell}{\mathrm{d}T}\right\|_\ell$ |
|---|---|---|---|
| $E_0$ | | 4.7 | 4.5 [5] |
| $(E_0+\Delta_0)_\mathrm{Ex}$ | 5.5 | 5 | |
| $(E_1)_\mathrm{2D}$ | 8.7 | 6.6 | |
| $(E_1)_\mathrm{Ex}$ | 6.9 | 6.2 | |
| $(E_1+\Delta_1)_\mathrm{2D}$ | 4.8 | 3.7 | |
| $(E_1+\Delta_1)_\mathrm{Ex}$ | | 7.9 | |

**Table 5.** Values of the parameters entering relation (5) giving the broadening parameter for each critical transition *versus* temperature. The last suffix in column 1 indicates the lineshape used for the fit of experimental data.

| Transition $\ell$ and fitting lineshape | $\Gamma_{\ell 1}$ (meV) | $\Gamma_{\ell 0}$ (meV) | $\Gamma'_\ell$ (T) | Error bar on $\Gamma_\ell$ (meV) |
|---|---|---|---|---|
| $E_0$ | 55.5 | 56.5 | 533 | $\pm 2$ |
| $(E_0+\Delta_0)_\mathrm{Ex}$ | 1.2 | 17.6 | 186 | $\pm 3$ |
| $(E_1)_\mathrm{2D}$ | 58.5 | 52.5 | 306 | $\pm 6$ |
| $(E_1)_\mathrm{Ex}$ | 38.5 | $8\times10^{-4}$ | 10 | $\pm 2$ |
| $(E_1+\Delta_1)_\mathrm{2D}$ | 143 | 3.1 | 32 | $\pm 4$ |
| $(E_1+\Delta_1)_\mathrm{Ex}$ | 55 | 3.3 | 45 | $\pm 3$ |

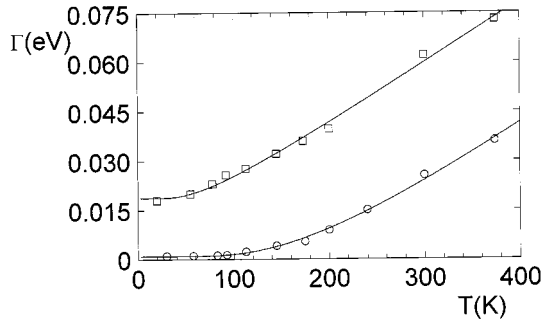


(a)

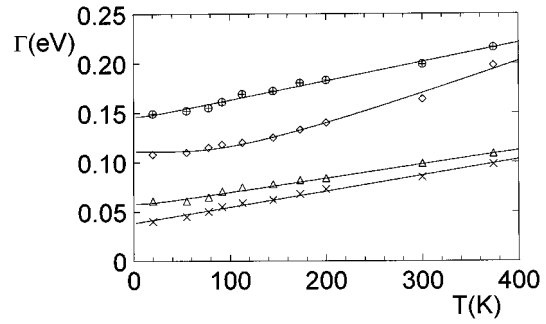


(b)

**Fig. 6.** (a) Temperature variations of the broadening parameters at $E_0$ and $E_0+\Delta_0$ with the same symbols as in Figure 7a. (b) Temperature variations of the broadening parameters at $E_1$ and $E_1+\Delta_1$ with the same symbols as in Figure 7b.

Fig. 2) below 200 K. $\varepsilon_\mathrm{i}$ goes down to a non measurable value 2 meV above the maximum of the first peak. The simultaneous fit of $\varepsilon_\mathrm{r}$ and $\varepsilon_\mathrm{i}$ spectra near $E_0$ with (2)+(3) gives correct values for the energies however this fit is misleading in the determination of the broadening parameters as the spectral width of the monochromator is dose to or larger than the broadening of the exciton states at least at low temperatures. To obtain more accurate values of the $\Gamma_{\mathrm{Ex},p}$ and of $\Gamma(E_0)$ we take into account the spectral shape of the transfer function of the monochromator. This function is assumed to be Lorentzian and is written:

$$H(E)=\frac{S}{1+4(E_\mathrm{M}-E)^2/(\Delta B)^2} \tag{6}$$

$S$ is the insertion loss of the monochromator which is not known, $\Delta B$ its spectral width (here 0.5 meV) and $E_\mathrm{M}$ the photon energy at the maximum of $H(E)$.

The convolution of (2) + (3) with (6) is calculated numerically and the parameters entering (2) and (3) are determined so as to obtain the best fit of $\varepsilon(E)$. The fit is limited to 100 meV above $E_0$ to stay in the parabolic approximation of the bands leading to relation (2). The binding energy $G$ of the exciton is 18.7 meV $\pm$ 0.3 meV. $G$ stays constant with $T$ up to 200 K where the contribution of the two upper states of the exciton merge with the continuum. Its value is very comparable to those already given in the literature [28,29]. For $T<120$ K, the phase angle $\phi(E_0)_\mathrm{Ex}$ has the value of $\pi/2\pm10°$ corresponding to 3D transitions of $M_0$ type between uncorralated states. This value shows that the continuum of states of the exciton do not change appreciably the symmetry in the density of states of the extended states very near above the fundamental gap. $\phi(E_0)_\mathrm{Ex}$ increases slowly to 120° at 200 K where the description by (3) + (2) becomes meaningless.

Above 200 K $\varepsilon(E)$ is very well described using only (2) with $n=-1$ corresponding to an exciton lineshape. If this expression is also used to describe $\varepsilon(E)$ for $T<200$ K the value of $\phi(E_0)_\mathrm{Ex}$ deduced from this fit is, of course, 180° in agreement with an excitonic transition. Near 100 K starts to decrease slowly with $T$ to reach 140° at 200 K and then 110° at 360 K. For $T>200$ K the deviation of $\phi(E_0)_\mathrm{Ex}$ from 180° is characteristic of the interaction of the exciton with the states of the bands above the fundamental gap. $\varepsilon(E)$ data have also been fitted with a pure 3D transition above 200 K. $\phi(E_0)_\mathrm{3D}$ remains far from the value $\pi/2$ corresponding to uncorrelated transitions even at 380 K where $\phi(E_0)_\mathrm{3D}=150°$. This result is in accordance with the criterion of negligible excitonic coupling which holds when $\Gamma(E_0)\gg 70$ G [31] and is far from being fulfilled as $\Gamma(E_0)_\mathrm{Ex}=36$ meV at this temperature (*cf.* Fig. 6a).

The energy of the band gap $E_0$ is found the same, within $\pm2$ meV, whatever the choice for the type of transition used (excitonic or 3D) and, if, obviously, an upward shift of the excitonic binding energy (18.7 meV)

is applied to the onset energy deduced when expression (2) is used alone for 3D transitions.

$E_0(T)$ variations, presented in Figure 5a, are described by relation (4) which parameters are given in Table 3. Temperature coefficients $\mathrm{d}E_0/\mathrm{d}T$ are then deduced and reported in Table 4 where they are compared with data of the literature. $E_0(T)$ is also fairly well described by the Varshni relation [30]:

$$E_0 = 2.8208 \text{ eV} - 7.5 \times 10^{-4} \times T^2/(T + 311 \text{ K}).$$

The parameters are close to those deduced by Tournie *et al.* [14] particularly the 0 K value of $E_0$ which is the same if the exciton binding energy is cut of in our expression and considering the uncertainty which is ±1 meV at 20 K.

The broadening of the fundamental state of the exciton $\Gamma_{\mathrm{Ex},1}$ is shown in Figure 6a for $T < 200$ K. The broadenings of the two upper states are slightly larger and increase with nearly the same law. Above 200 K only one exciton lineshape can be used to describe $\varepsilon(E)$. The broadenings $\Gamma(E_0)_{\mathrm{Ex}}$ which are so deduced fit together very well those of the fundamental state of the exciton $\Gamma_{\mathrm{Ex},1}$ for $T < 200$ K. The continuity in the variation of the $\Gamma$ deduced in the two different temperature domains and with two different expressions is related to the high level contribution of the fundamental state of the exciton to the dielectric function both at low temperature where two upper states are seen but also at high temperatures where the $E_0$ transition remains governed by the exciton up to 380 K. These broadening values are reported in Figure 6a and used to set up an expression $\Gamma(E_0)_{\mathrm{Ex}}(T)$. The corresponding parameters entering (5) are given in Table 5.

Below 200 K the broadening $\Gamma(E_0)_{\mathrm{3D}}$ associated to 3D uncorrelated transitions, which is not drawn, increases drastically from 10 meV at 20 K to 242 meV at 200 K. Its low temperature value is comparable to those of transitions between bands (*cf.* $\Gamma(E_1)$ and $\Gamma(E_1 + \Delta_1)$ for instance). Its high value above 100 K may be due to the model itself which does not take into account the interaction between the exciton states and the continuum of the bands.

### 4.2 $E_0 + \Delta_0$ transition

$E_0 + \Delta_0$ is a weak transition between $\Gamma_7^{\mathrm{v}}$ and $\Gamma_6^{\mathrm{v}}$ states. It is however clearly seen in the $\varepsilon_{\mathrm{r}}$ and $\varepsilon_{\mathrm{i}}$ spectra shown in Figures 1 and 2. This transition is studied with the SCP model using both excitonic or 3D transitions. Below 100 K the excitonic lineshape describes very well this transition, the phase angle $\phi(E_0 + \Delta_0)_{\mathrm{Ex}}$ stays at the value 180° within ± 3° confirming the excitonic character of this transition. $\phi(E_0 + \Delta_0)_{\mathrm{Ex}}$ decreases with temperature as seen in Figure 7. This decrease above 100 K indicates that the bound state interacts with the continuum. In return the phase angle $\phi(E_0 + \Delta_0)_{\mathrm{Ex}}$ deduced from the fit with a 3D lineshape decreases from 220° at 20 K to 160° at 380 K. $\phi(E_0 + \delta_0)_{\mathrm{3D}}$ values are far from $\pi/2$ corresponding to a $M_0$ type for transition between uncorrelated states. At 380 K the coulomb interaction remains important and the results given here are those deduced from a fit with the exciton lineshape.

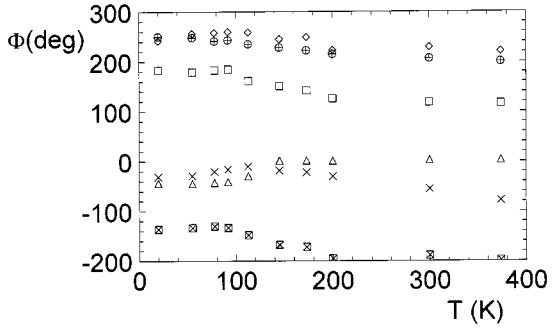


**Fig. 7.** Temperature variations of the phase angle $\phi$, symbols meanings are those of Figures 7a and 7b, (⊕) broadening at $E_0 + \Delta_0$ with a 3D lineshape.

The spin orbit splitting $\Delta_0$ is deduced from the energies of the two transitions studied. $\Delta_0$ stays constant with $T$ up to 100 K at the value of $0.418 \pm 0.005$ eV. It then decreases to 0.408 eV when $T$ increase to 380 K with a law very similar to that of $\phi(E_0)_{\mathrm{Ex}}$ or $\phi(E_0 + \delta_0)_{\mathrm{Ex}}$. This decrease of $\Delta_0$ appears surprising as this energy originates essentially from an intra-atomic spin orbit interaction [32]. Such a decrease with $T$ is also found for CdTe [33]. We verified that its origin is the same and rests on a choice of the same lineshapes for the fits in the whole temperature range, here the exciton lineshape both for $E_0$ and $E_0 + \Delta_0$ above 200 K. The values of $E_0$ and $E_0 + \Delta_0$ are deduced at high temperature with an exciton lineshape in a temperature domain where the transitions do not correspond to pure excitons. The most accurate value of $\Delta_0$ are those deduced at low temperatures. A mean value between six data taken at six temperatures gives $\Delta_0 = 0.418 \pm 0.005$ eV. With this conclusion $\mathrm{d}(E_0 + \Delta_0)/\mathrm{d}T = \mathrm{d}E_0/\mathrm{d}T$ and is not discussed further. The broadening parameter $\Gamma(E_0 + \Delta_0)_{\mathrm{Ex}}$ appears likely more accurate than that deduced with a 3D lineshape which is found lower than 3 meV at low temperatures. $\Gamma(E_0 + \Delta_0)_{\mathrm{Ex}}$ variations with $T$ are drawn in Figure 6a and the parameters of (5) describing them are given in Table 5.

### 4.3 $E_1$ transition

This strong transition links $\mathrm{L}_{0.45}^{\mathrm{v}}$ and $\mathrm{L}_6^{\mathrm{c}}$ states but also states along $\Lambda(\Lambda_{4.5}^{\mathrm{v}} \rightarrow \Lambda_6^{\mathrm{c}})$ direction where the joint density of states is high. The asymmetry of the ZnSe $\varepsilon_{\mathrm{i}}(E)$ spectrum around $E_1$ at 10 K has been explained by the effect of the Coulomb interaction at this saddle point [10]. Since this date it is a general use to consider a high Coulomb interaction at such transitions [7,12,19,20]. In return Kim and Sivanathan claim the $\varepsilon(E)$ is very well described in the vicinity of $E_1$ if only uncorrelated transitions (of 2D type) are considered [8]. However the number of fitting parameters to experimental data entering their

model is high and their values cannot reveals the nature of involved transitions. The number of parameters entering the usual SCP model is relatively low and the most important parameter is the phase angle $\phi(E_1)$ and is related to the asymmetry of $\varepsilon_r(E)$. The SCP model seems to be the simplest one giving an estimation about the Coulomb correlation at the $E_1$ transition. $\varepsilon_r(E)$ and $\varepsilon_i(E)$ are fitted simultaneously with a 2D lineshape on the one hand and with an exciton lineshape on the other hand. The results of the fits are now discussed.

The fit itself with the exciton lineshape performed on the second derivatives of $\varepsilon_r(E)$ and $\varepsilon_i(E)$ is a little closer to the experimental derivatives than that with a 2D lineshape particularly at low temperatures and especially in the wings of the oscillations on each side of $E_1$ (*cf.* Fig. 3). However the difference in the confidence number, which is a mean of the squares of the difference between calculated and experimental values of $\varepsilon_r$ and $\varepsilon_i$, do not allow to assess that the choice of one lineshape is better than the other. $\phi(E_1)_{Ex}$ variations with $T$, which are drawn in Figure 7, have a small decrease between 20 K and 380 K, however their values stay appreciably above that of a pure exciton ($\phi_{Ex} = \pi$). This is often described as resulting from an interaction of the bound state with the continuum states. But we see also in Figure 3 that, if the decrease of $\phi(E_1)_{2D}$ is higher, it goes toward $3\pi/2$ at high temperatures. This value of the phase angle corresponds well to that of uncorrelated transitions at a saddle point [20] which are expected as the joint density of states along the $\Lambda$ direction in the Brillouin zone is very high [27]. High values of $\phi(E_1)_{Ex}$ express an asymmetric part in the $\varepsilon_i(E)$ variation just above $E_1$ which is not very pronounced (see Fig. 2). This asymmetry can be attributed to correlation effects, their contributions to $\varepsilon(E)$ remain almost independent of $T$. However, at high temperatures and at 300 K, $\varepsilon(E)$ is very well described with a 2D lineshape at a saddle point [8]. The oscillator strength $C(E_1)$ in (2) has nearly the same decrease with $T$ whatever is the lineshape used and tells us that these transitions are not of pure excitonic nor 2D type. $E_1$ values deduced from both lineshapes are equal within $\pm 6$ meV for $T < 160$ K. Above 160 K, the $(E_1)_{2D}$ decrease with $T$ is slightly higher than that of $(E_1)_{Ex}$. Both values agree well with those already given in the literature [23]. $E_1$ variations are well described by expression (4) and the parameter values deduced for both lineshapes are gathered in Table 3. The corresponding temperature coefficients which can be deduced are given in Table 4. The broadening parameter depends strongly on the lineshape used for the fit. As both lineshapes can describe $\varepsilon(E)$ fairly well near $E_1$, both variations are drawn in Figure 6b. In the same way the parameters entering relation (5) are given in Table 5 for both lineshapes.

### 4.4 $E_1 + \Delta_1$ transition

This transition links $L_6^v$ and $L_6^c$ states but also states along the $\Lambda_6$ direction in the Brillouin zone. It is of the same type as the transition $E_1$; however $E_1 + \Delta_1$ is on the high energy side of the strong $E_1$ transition (*cf.* Fig. 1) in a domain of decreasing sensitivity of the ellipsometer.

$\phi(E_1 + \Delta_1)_{Ex}$ variations with $T$, reproduced in Figure 7, are near to those of confirming the preceeding statement. $\phi(E_1 + \Delta_1)_{Ex}$ has a variation with $T$ opposite to that (*cf.* Fig. 7) and remains remarkably constant at $0°$ for $T > 140$ K. This value corresponds to a maximum which is not likely for this transition. $E_1 + \Delta_1$ determinations remain the same within $\pm 6$ meV up to 160 K. Above this temperature $(E_1 + \Delta_1)_{2D}$ has a lower decrease with $T$ than $(E_1 + \Delta_1)_{Ex}$ which is opposite to the $E_1(T)$ variation as can be seen in Figure 5b.

The difference $(E_1 + \Delta_1)_{Ex} - (E_1)_{Ex} = (\Delta_1)_{Ex}$ decreases smoothly with $T$ from the 30 K value of 0.273 eV. $\phi(E_1)_{2D}$ has a lower 20 K value of 0.256 eV but then increases with $T$ steeper than $(E_1)_{Ex}$. Here also the difference in the determination of $\Delta_1$ which increases with $T$ depends on the choices of lineshapes in a temperature domain where they do not strictly apply [33]. The low temperature determinations are probably the most accurate ones and we propose to take $\Delta_1 = 0.260 \pm 0.007$ eV which is the mean value on data obtained at temperatures lower than 100 K and using both lineshape fittings. $\Delta_1$ originates from an intra atomic coupling and must stay independent with temperature so $E_1 + \Delta_1$ variations with $T$ are the same as those of $E_1$ which have been already given.

The broadening parameter $\Gamma(E_1 + \Delta_1)_{Ex}$ is obviously larger than $\Gamma(E_1 + \Delta_1)_{2D}$ but both have an almost linear variation with $T$ as seen in Figure 6b.

## 5 Conclusion

Ellipsometric measurements performed between 20 K and 380 K allow the study of the temperature behaviour of the four transitions of ZnSe seen from the fundamental gap $E_0$ up to 5.5 eV. Temperature variations of the energies $E_0$, $E_0 + \Delta_0$, $E_1$ and $E_1 + \Delta_1$ are given and studied with the standard critical point model.

At low temperatures and near the fundamental gap, the dielectric function is dominated by the exciton contribution. For the first time, an ellipsometric measurement shows the fundamental state of the exciton completely separated from its excited states showing the high resolution reached by ellipsometric measurements.

The experimental results are analysed and interpreted at each critical energy point.

The transitions near $E_1$ and $E_1 + \Delta_1$ are not of pure 2D or excitonic type but rather correspond to a quasi bound state interacting with continuum states in the whole temperature range. Thus the dielectric response can be fairly well described by both lineshapes. The small amplitude variations with temperature of the spin orbit splitting $\Delta_0$ and $\Delta_1$ are explained by the use of lineshapes for the fits which can be strictly applied for pure transitions only.

## References


1. M.A. Haase, J. Qiu, J.M. De Puydt, H. Cheng, Appl. Phys. Lett. **59**, 1272 (1991).
2. J.M. Depuydt, M.A. Haase, J. Qiu, H. Cheng, J. Cryst. Growth **117**, 1078 (1992).
3. A. Feldman, D. Horwitz, R. Waxler, M. Dodge, Technical Note 993 (1979) National Bureau of Standards.
4. A.R. Hilton Sr., Proc. SPIE (USA) **1307**, 516 (1990).
5. H.E. Gumlich, D. Theis, D. Tschierse, in *Landolt-Börnstein Numerical data*, **17**, 126 (1982).
6. L. Ward, in *Handbook of Optical Constants of Solids II*, edited by E.D. Palik (Acad. Press, Orlando, 1991), p. 743.
7. S. Adachi, T. Taguchi, Phys. Rev. B **43**, 9569 (1991).
8. C.C. Kim, S. Sivanathan, Phys. Rev. B **53**, 1475 (1996).
9. C.C. Kim, J.W. Garland, H. Abad, P.M. Raccah, Phys. Rev. B **45**, 11749 (1992).
10. Y. Petroff, M. Balkanski, Phys. Rev. B **3**, 3299 (1971).
11. O. Castaing, J.T. Benhlal, R. Granger, accepted in the European Physical Journal B.
12. M. Cardona, *Modulation spectroscopy*, Solid State Phys. Supl. **11** (Academic Press, New-York, 1969).
13. R. Triboulet, J.O. Ndap, A. Tromson-Carli, P. Lemasson, C. Morhain, G. Neu, J. Cryst. Growth **159**, 156 (1996).
14. E. Tournié, C. Morhain, G. Neu, M. Laügt, C. Ongarette, J.P. Faurie, R. Triboulet, J.O. Ndap, J. Appl. Phys. **80**, 2983 (1996).
15. Y.D. Kim, S.L. Cooper, M.L. Klein, Appl. Phys. Lett. **62**, 2387 (1993).
16. R.M. Azzam, N.M.A. Bashara, *Ellipsometry and polarized light* (North Holland, Amsterdam, 1977).
17. L. Viña, S. Logotheditis, M. Cardona, Phys. Rev. B **30**, 1979 (1984).
18. S. Zollner, Appl. Phys. Lett. **63**, 2523 (1993).
19. P. Lautenschlager, M. Garriga, L. Viña, M. Cardona, Phys. Rev. B **36**, 4821 (1987).
20. D.E. Aspnes, *Handbook of Semiconductors*, edited by M. Balkanski, (North-Holland, Amsterdam, 1980), Vol. 2.
21. J.W. Garland, C.C. Kim, H. Abad, P.M. Raccah, Thin Solid Films **233**, 148 (1993).
22. W.H. Press, B.P. Flannery, S.A. Tenkolsky, W.T. Vetterling, *Numerical Recipes, the Art of Scientific Computing* (Cambridge University Press, 1989), p. 523.
23. H.E. Gumlich, D. Theis, D. Tschierse, in *Landolf-Börnstein series*, Vol. 17 (Springer Verlag, 1982), p. 388.
24. R.J. Elliott, Phys. Rev. **108**, 1384 (1957).
25. M.L. Cohen, D.J. Chadi, in [20] p. 155.
26. Y.P. Varshni, Physica **34**, 149 (1967).
27. J. Chelikowsky, M.L. Cohen, Phys. Rev. B **14**, 556 (1976).
28. H. Veughaus, Phys. Rev. B **19**, 3071 (1979).
29. G.N. Aliev, R.M. Datsiev, S.V. Ivanov, P.S. Ko'ev, R.P. Seisyan, S.V. Sorokin, J. Cryst. Growth **159**, 523 (1996).
30. Y.P. Varshni, Physica **34**, 149 (1967).
31. V.A. Tagai, O.V. Snitko, V.N. Bondarenko, N.I. Vitrikhorskii, V.B. Popov, A.N. Krasiko, Soviet Phys. Solid State **16**, 885 (1974).
32. P. Lautenschlager, M. Garriga, S. Logotheditis, M. Cardona, Phys. Rev. B **35**, 9174 (1987).
33. J.T. Benhlal, K. Strauch, R. Granger, R. Triboulet, Optic. Mater. **12**, 143 (1999).
34. G. Bruhat, *Cours de Physique Générale* (édition Masson et Cie, 1959), Chap. XIX.